G. Vasquez, S. Lee, T. P. Prakash, E. V. Wancewicz, D. Witchell and E. E. Swayze, *J. Med. Chem.*, 2009, **52**, 10; (*c*) T. P. Prakash, A. Siwkowski, C. R. Allerson, M. T. Migawa, S. Lee, H. J. Gaus, C. Black, P. P. Seth, E. E. Swayze and B. Bhat, *J. Med. Chem.*, 2010, **53**, 1636; (*d*) P. P. Seth, C. R. Allerson, A. Berdeja, A. Siwkowski, P. S. Pallan, H. Gaus, T. P. Prakash, A. T. Watt, M. Egli and E. E. Swayze, *J. Am. Chem. Soc.*, 2010, **132**, 14942; (*e*) P. P. Seth, G. Vasquez, C. A. Allerson, A. Berdeja, H. Gaus, G. A. Kinberger, T. P. Prakash, M. T. Migawa, B. Bhat and E. E. Swayze, *J. Org. Chem.*, 2010, **75**, 1569; (*f*) K. Miyashita, S. M. A. Rahman, S. Seki, S. Obika and T. Imanishi, *Chem. Commun.*, 2007, 3765.

8 J. Lietard and C. J. Leumann, *J. Org. Chem.*, 2012, **77**, 4566.

9 A. Yahara, A. R. Shrestha, T. Yamamoto, Y. Hari, T. Osawa, M. Yamaguchi, M. Nishida, T. Kodama and S. Obika, *ChemBioChem*, 2012, **13**, 2513.

10 (*a*) M. W. Johannsen, L. Crispino, M. C. Wamberg, N. Kalra and J. Wengel, *Org. Biomol. Chem.*, 2011, **9**, 243; (*b*) S. K. Singh, R. Kumar and J. Wengel, *J. Org. Chem.*, 1998, **63**, 6078; (*c*) M. D. Sorensen, M. Petersen and J. Wengel, *Chem. Commun.*, 2003, 2130.

11 K. Mori, T. Kodama, T. Baba and S. Obika, *Org. Biomol. Chem.*, 2011, **9**, 5272.

12 (*a*) Y. Mitsuoka, T. Kodama, R. Ohnishi, Y. Hari, T. Imanishi and S. Obika, *Nucleic Acids Res.*, 2009, **37**, 1225; (*b*) M. Nishida, T. Baba, T. Kodama, A. Yahara, T. Imanishi and S. Obika, *Chem. Commun.*, 2010, **46**, 5283; (*c*) K. Morita, M. Takagi, C. Hasegawa, M. Kaneko, S. Tsutsumi, J. Sone, T. Ishikawa, T. Imanishi and M. Koizumi, *Bioorg. Med. Chem.*, 2003, **11**, 2211; (*d*) Y. Liu, J. Xu, M. Karimiahmadabadi, C. Zhou and J. Chattopadhyaya, *J. Org. Chem.*, 2010, **75**, 7112; (*e*) A. R. Shrestha, Y. Kotobuki, Y. Hari and S. Obika, *Chem. Commun.*, 2014, **50**, 575.

13 M. Egli, G. Minasov, M. Teplova, R. Kumar and J. Wengel, *Chem. Commun.*, 2001, 651.

14 T. Yamamoto, S. Obika, M. Nakatani, H. Yasuhara, F. Wada, E. Shibata, M. A. Shibata and M. Harada-Shiba, *Eur. J. Pharmacol.*, 2014, **723**, 353.

15 T. Yamamoto, N. Fujii, H. Yasuhara, S. Wada, F. Wada, N. Shigesada, M. Harada-Shiba and S. Obika, *Nucleic Acid Ther.*, 2014, **24**, 283.

16 (*a*) T. Yamamoto, M. Harada-Shiba, M. Nakatani, S. Wada, H. Yasuhara, K. Narukawa, K. Sasaki, M. A. Shibata, H. Torigoe, T. Yamaoka, T. Imanishi and S. Obika, *Mol. Ther. Nucleic Acids*, 2012, **1**; (*b*) R. Z. Yu, B. Baker, A. Chappell, R. S. Geary, E. Cheung and A. A. Levin, *Anal. Biochem.*, 2002, **304**, 19.

This journal is © The Royal Society of Chemistry 2015

NUCLEIC ACID THERAPEUTICS
Volume 24, Number 4, 2014
© Mary Ann Liebert, Inc.
DOI: 10.1089/nat.2013.0470

Brief Communication

Evaluation of Multiple-Turnover Capability of Locked Nucleic Acid Antisense Oligonucleotides in Cell-Free RNase H-Mediated Antisense Reaction and in Mice

Tsuyoshi Yamamoto,[1] Naoko Fujii,[1] Hidenori Yasuhara,[1] Shunsuke Wada,[1] Fumito Wada,[1] Naoya Shigesada,[1] Mariko Harada-Shiba,[2] and Satoshi Obika[1]

The multiple-turnover ability of a series of locked nucleic acid (LNA)-based antisense oligonucleotides (AONs) in the RNase H-mediated scission reaction was estimated using a newly developed cell-free reaction system. We determined the initial reaction rates of AONs under multiple-turnover conditions and found that among 24 AONs tested, AONs with melting temperatures (*T*m) of 40°C–60°C efficiently elicit multiple rounds of RNA scission. On the other hand, by measuring *T*m with two 10-mer RNAs partially complementary to AONs as models of cleaved 5′ and 3′ fragments of mRNA, we found that AONs require adequate binding affinity for efficient turnover activities. We further demonstrated that the efficacy of a set of 13-mer AONs in mice correlated with their turnover efficiency, indicating that the intracellular situation where AONs function is similar to multiple-turnover conditions. Our methodology and findings may provide an opportunity to shed light on a previously unknown antisense mechanism, leading to further improvement of the activity and safety profiles of AONs.

Introduction

ANTISENSE OLIGONUCLEOTIDES (AONs) having specific configurations compatible with RNase H-inducible capacity have been developed over decades and have been shown to be very powerful and robust gene silencing materials in cultured cells and animals, as well as in humans (Crooke, 2007; Yamamoto et al., 2011). In particular, the "gapmer" configuration, which is a chimeric AON consisting of a central RNase H-recruitable DNA stretch pinched by affinity-enhancing modified nucleic acids with fully phosphorothioated (PS) internucleotide linkages, has shown great promise. Affinity-enhancing modified nucleic acids, such as MOE (2′-*O*-methoxyethyl RNA), 2′,4′-BNA/LNA (2′-*O*,4′-*C*-methylene bridged nucleic acid/locked nucleic acid) (Fig. 1A) (Obika et al., 1997; Obika et al., 1998; Singh et al., 1998), and other bridged nucleic acids (BNAs) (Hari et al., 2006; Miyashita et al., 2007; Seth et al., 2009; Prakash et al., 2010; Yahara et al., 2012) mostly interfere with RNase H activity, but when used in a chimeric gapmer, they assist in enhancing target binding and nuclease stability, greatly improving its potency without affecting RNase H capacity. Despite these innovations, very few products have been released on the market and some candidates in clinical trials have been dropped due to efficacy and safety issues.

More recently, Straarup et al. successfully improved efficacy of an earlier LNA-based gapmer targeting apolipoprotein B-100 (apoB) by trimming its conventional long-strand [16∼20 nucleotides (nt)] and utilizing the resulting shorter LNA gapmers (∼13 nt) (Straarup et al., 2010). Our group also independently reproduced and extended this observation by using newly developed 2′,4′-BNA^{NC} chemistry and supported the unusual notion that a drug with weaker binding has stronger silencing activity (Fig. 1A) (Yamamoto et al., 2012b). One possible explanation for this finding is that shorter AONs accelerate the reaction to a greater degree than conventional AONs *via* turnover mechanisms. Stanton et al. recently observed that melting temperatures (*T*m) of greater than 80°C showed reduced silencing activity and explained this finding as a result of an inability to recycle AONs in cells (Stanton et al., 2012). However, to the best of our knowledge, there is no experimental evidence of AON turnover, despite its anticipated importance as in RNAi mechanisms (Hutvagner and Zamore, 2002). If turnover of AONs was demonstrated in antisense mechanisms, a more favorable configuration or chemistry that accelerates AON turnover may be discovered, and this discovery could lead to additional insights into strategies for further improving the activity and safety of AONs. Most previous works related to antisense reaction kinetics have been conducted to determine whether duplexes of interest have an ability to elicit RNase H, and are thus performed under excess amounts of AON/RNA duplex over RNase H in cell-free systems (single-turnover conditions for AON) (Crooke et al., 1995; Lima and Crooke,

[1]Graduate School of Pharmaceutical Sciences, Osaka University, Suita, Osaka, Japan.
[2]Department of Molecular Innovation in Lipidology, National Cerebral and Cardiovascular Center Research Institute, Suita, Osaka, Japan.

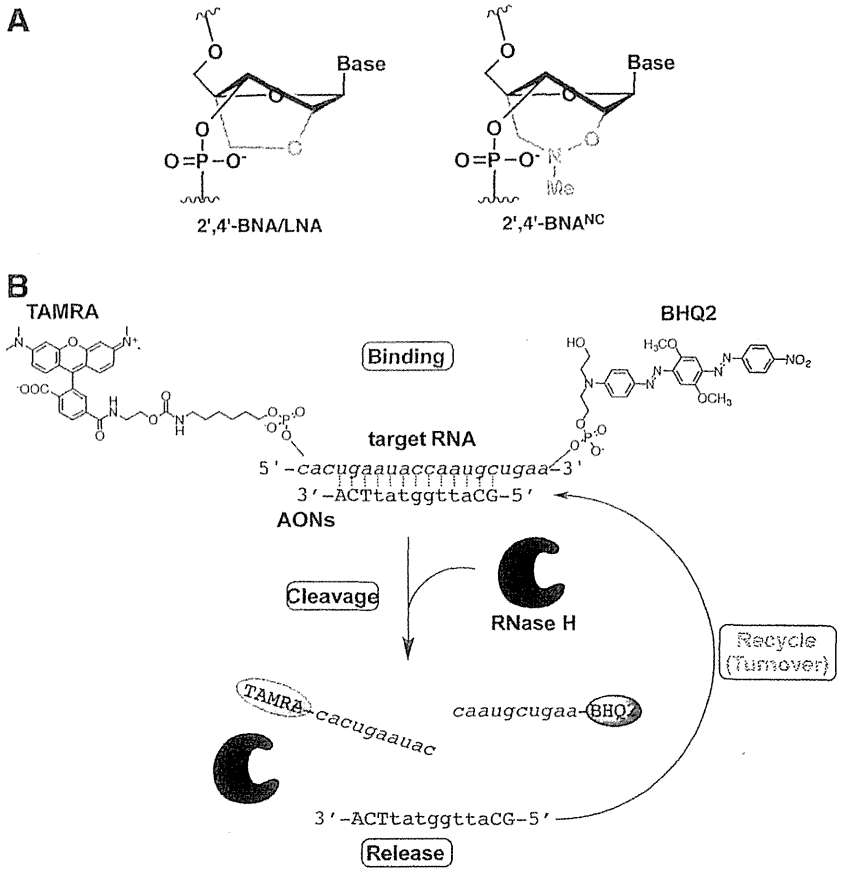

FIG. 1. Recycling of antisense oligonucleotides in antisense reaction. (**A**) Structures of bridged nucleic acids (BNAs). (**B**) Schematic illustration of cell-free Förster resonance energy transfer (FRET)-based turnover monitoring system used in this study. Color images available online at www.liebertpub.com/nat

1997; Vester et al., 2008; Stanton et al., 2012). In the present study, to investigate whether AONs are recyclable in antisense reactions, we devised a cell-free reaction system, in which synthetic 20-mer target RNA conjugated with a pair of FRET (Förster resonance energy transfer) dyes and *Escherichia coli*–derived RNase H are both in excess over AONs (multiple-turnover conditions). In this system, an increase in fluorescence from the FRET donor is observed after binding, cleavage, and release proceeds sequentially (Fig. 1B). The main problem facing previous works is the potential difficulty in separating affinity issues from length issues, because affinity usually varies as a function of strand length. In this study, we utilized LNA, which enables us to freely modify AON affinity without changing length; thus, we prepared a series of LNA-based apoB-targeting AONs with a central focus on 13-mer AONs (Table 1), one of which (ApoB-13a) had been previously characterized as highly potent *in vitro* and *in vivo* (Straarup et al., 2010; Yamamoto et al., 2012b).

Materials and Methods

Oligonucleotides

All oligonucleotides listed in Table 1 were purchased from Gene Design Inc.

Thermal denaturation experiments

Thermal denaturation experiments were carried out on SHIMADZU UV-1650 and UV-1800 spectrometers equipped with a *T*m analysis accessory. For duplex formation, equimolecular amounts of target RNA and each AON were dissolved in 10 mM sodium phosphate buffer (pH = 7.2) containing 100 mM (1.0 M for MRNA-1, MRNA-2) NaCl to give a final strand concentration of 2.0 μM. Duplex samples were then annealed by heating at 90°C, followed by slow cooling to room temperature. Melting profiles were recorded at 260 nm from 0°C to 95°C at a scan rate of 0.5°C/minute. Melting temperatures were obtained as maxima of the first derivative of the melting curves.

Turnover experiments

Dual-labeled complementary RNA probe (DL-MRNA) and non-labeled complementary 20-mer RNA (NL-MRNA) were combined in a 1:3 molar ratio. The intended amounts of the resulting mixture and AON were added to RNase H reaction buffer (New England Biolabs). The reaction was initiated by addition of 1 μL of the intended concentrations of *E. coli* RNase H (Takara) to 199 μL of reaction mixture. Fluorescence intensity was recorded once every 15 seconds for 15 minutes at 555 nm (ex) and 590 nm (em) using a fluorescence microplate reader (Molecular Devices). The initial turnover rates ($v0$) were calculated by fitting a linear regression line to the data for the first 0–60 seconds and then converted the resulting slopes expressed as RFU/second into $v0$ (nM/second) by using a conversion factor, 6.15 (RFU/nM), determined by experiments shown in Supplementary Fig. S1 (Supplementary Data are available online at www.liebertpub.com/nat).

TABLE 1. OLIGONUCLEOTIDES USED IN THIS STUDY

No.	*Sequence ID*	*Sequence*	T_m (°C)
1	**ApoB-20a**	5′-TTCAGcattggtattCAGTG-3′	76 ± 0.4
2	**ApoB-20b**	5′-T°T°C°A°Gcattggtatt C°A°G°T°G-3′	79 ± 0.6
3	**ApoB-20c**	5′-t°t°c°a°g°c°a°t°t°g°g°t°a°t°t°c°a°g°t°g-3′	59 ± 0.6
4	**ApoB-16a**	5′-CAGcattggtatTCAG-3′	66 ± 0.5
5	**ApoB-14a**	5′-AGCattggtatTCA-3′	62 ± 0.6
6	**ApoB-14b**	5′-AgCattggtatTcA-3′	58 ± 0.4
7	**ApoB-13a**	5′-GCattggtatTCA-3′	59 ± 0.5
8	**ApoB-13b**	5′-G°Cattggtat T°C°A-3′	62 ± 0.1
9	**ApoB-13c**	5′-gCattGgtatTCA-3′	63 ± 0.5
10	**ApoB-13d**	5′-GcattggtaTTCA-3′	58 ± 0.8
11	**ApoB-13e**	5′-GCattggtattCA-3′	55 ± 0.5
12	**ApoB-13f**	5′-G°CattggtattC°A-3′	57 ± 0.1
13	**ApoB-13g**	5′-GCattggtatTcA-3′	58 ± 0.6
14	**ApoB-13h**	5′-gcattggtatTCA-3′	48 ± 0.7
15	**ApoB-13i**	5′-GCAttggtattca-3′	50 ± 0.5
16	**ApoB-12a**	5′-GCattggtatTC-3′	52 ± 0.6
17	**ApoB-12b**	5′-GCattggtaTtC-3′	53 ± 0.5
18	**ApoB-12c**	5′-G°CattggtatT°C-3′	54 ± 0.5
19	**ApoB-11a**	5′-CAttggtatTC-3′	39 ± 0.5
20	**ApoB-11b**	5′-C°AttggtatT°C-3′	41 ± 0.4
21	**ApoB-10a**	5′-CattggtatT-3′	28 ± 0.4
22	**ApoB-10b**	5′-CAttggtaTT-3′	33 ± 0.6
23	**ApoB-10c**	5′-C°AttggtaT°T-3′	36 ± 0.5
24	**ApoB-10d**	5′-cattggtATT-3′	29 ± 0.5
25	**DL-MRNA**	5′-R-*cacugaauaccaaugcugaa*-Q-3′	
26	**NL-MRNA**	5′-*cacugaauaccaaugcugaa*-3′	
27	**MRNA-1**	5′-*cacugaauac*-3′	
28	**MRNA-2**	5′-*caaugcugaa*-3′	

Upper case, *lower case*, *lower italic*, and *superscript circle* indicate locked nucleic acid (LNA), DNA, RNA, and phosphodiester linkage, respectively. All internucleotide linkages are phosphorothioated unless otherwise noted. All RNAs numbered 25, 26, 27, and 28 have phosphodiester internucleotide linkages. Melting temperatures (T_m) are shown as mean ± SD.

apoB, apolipoprotein B-100; dl-mrna, dual-labeled complementary RNA probe; nl-mrna, non-labeled complementary 20-mer RNA.

In vivo *pharmacological experiments*

All animal procedures were performed in accordance with the guidelines of the Animal Care Ethics Committee of the National Cerebral and Cardiovascular Center Research Institute. All animal studies were approved by an institutional review board. All C57BL/6J mice (CLEA Japan) were male, and studies were initiated when animals were 8 weeks of age. Mice were maintained on a 12-hour light/12-hour dark cycle and fed *ad libitum*. Mice received a single treatment of AONs administered subcutaneously at a dose of 0.75 mg/kg. At the time of sacrifice, mice were anesthetized and livers were harvested and snap frozen until subsequent analysis. Whole blood was collected and subjected to serum separation for subsequent analysis.

mRNA quantification

Total RNA was isolated from mouse liver tissues using TRIzol Reagent (Life Technologies Japan) in accordance with the manufacturer's instructions. Gene expression was evaluated using a two-step quantitative reverse transcription-polymerase chain reaction (RT-PCR) method. Reverse transcription of RNA samples was performed using a High-Capacity cDNA Reverse-Transcription Kit (Life Technologies), and quantitative PCR was performed using TaqMan Gene Expression Assays (Life Technologies Japan). Messenger RNA levels of apoB were normalized against GAPDH mRNA levels. For murine apoB and GAPDH, TaqMan gene expression assays were used (assay IDs: Mm01545156_m1 and Mm99999915_g1, respectively).

AON quantification in liver

Assay was performed as described previously (Yamamoto et al., 2012a). Template DNA: 5′-gaatagcgatgaataccaatgc-3′ with biotin at the 3′ end; ligation probe DNA: 5′-tcgctattc-3′ with phosphate at the 5′ end and digoxigenin at the 3′ end.

Serum chemistry

Assay kits (#439-17501; WAKO) were used to measure serum levels of total cholesterol.

Statistics

Pharmacological studies were performed with more than three mice per treatment group. All data are expressed as means ± standard deviation (SD). $P < 0.05$ was considered to be statistically significant in all cases. Statistical comparisons were performed by Dunnett's or Bonferroni's multiple comparison tests.

Results and Discussion

Our first goal was to prepare bioactive AONs with a variety of binding affinities for the target RNA. We designed and

synthesized 24 AONs, as shown in Table 1. Most of the AONs were 10- to 20-mer LNA/DNA chimeras with full or partial PS backbones. DNA stretches on these AONs were kept in the 6- to 10-nt range, which is expected to be sufficient for eliciting RNase H of both *E. coli* and mammalian origins (Monia et al., 1993; Kurreck et al., 2002). ApoB-13c containing LNA in the center of the gap was prepared as a non-cleavable negative control. We next determined *T*m values of all AONs with the NL-MRNA (Table 1). As expected, *T*m values of these AONs were uniformly and broadly distributed from approximately 30° to 80°C under the indicated buffer conditions.

In order to investigate turnover activities of AONs, we developed a cell-free fluorescent turn-on system. DL-MRNA labeled with reporter dye (TAMRA) and quencher (BHQ2) on the 5′ and 3′ termini, respectively, was designed and prepared to detect RNA scission. Using this probe, we first evaluated the turnover activity of previously validated ApoB-13a. In the presence of an 80- to 240-fold molar excess of complementary RNA, 10 nM ApoB-13a was pre-incubated at 37°C in a 96-well microplate before addition of RNase H. It should be noted that the target complementary RNA used here consists of one-quarter dual-labeled DL-MRNA and three-quarters non-labeled NL-MRNA to avoid undesirable quenching or other interactions that may affect fluorescence (Supplementary Table S1). After addition of 60 units per well RNase H to the reactions, fluorescence intensities of TAMRA were measured (excitation = 555 nm and emission = 590 nm) every 15 seconds for 15 minutes (Supplementary Fig. S1A). Fluorescence of the reporter dye increased over time. The initial reaction rates also increased as a function of RNA concentration, where the initial reaction rates were determined from the slope of the initial linear portions (0–60 seconds) of the plots of fluorescence intensity versus time. In contrast, time-dependent fluorescence changes in TAMRA were not seen in an ApoB-13a-lacking control. We also observed very low background fluorescence levels in the control group, which indicates efficient quenching of TAMRA fluorescence by BHQ2, despite these dyes being 20 nt distant from one another. The fluorescence increases reached a plateau at 5 minutes. We confirmed that this indicates the completion of degradation of all target RNAs and then attempted to estimate the conversion coefficient between fluorescence intensity and concentration of RNA (Supplementary Figs. S1B, S2). By plotting fluorescence intensities at 15 minutes as a function of RNA concentration, we found high linear correlations between fluorescence intensity and concentration and determined 6.15 (RFU/nM) as a conversion factor. To determine the required amount of RNase H in this system, we performed further tests with various amounts of RNase H (2–180 units/well). A near maximum reaction rate could be obtained when at least 60 units/well of RNase H were added to the reaction, and confirmed that the rate-determining step of this reaction was not the scission step, but was the recycling step under these conditions (Supplementary Fig. S3). Taken together, these results are consistent with the recycling of ApoB-13a during this cell-free antisense reaction (see also Supplementary Fig. S4; Supplementary Table S2), and this system is useful for rapid screening of multiple-turnover activities of a series AONs.

We next aimed to measure a set of initial rates of AONs (Table 1). The initial velocities were determined as described above. At a concentration of 10 nM, each AON was incubated in the presence of 800 nM complementary RNA (DL-MRNA:NL-MRNA = 1:3) and 60 units/well RNase H. Time-dependent fluorescence changes were measured and initial rates were subsequently determined. The observed initial rates were rearranged in ascending order of *T*m values of corresponding AONs and are shown in Fig. 2A. As expected, we found an inverted U-shaped relationship between initial rate and *T*m values on the whole: AONs with high (> 60°C) and low (< 30°C) *T*m values have relatively small initial rates, while AONs having *T*m of 40°C–60°C showed efficient turnover in this system. This implies that AONs having higher multiple-turnover activities are more potent than conventional long LNA gapmers with extraordinarily high affinity. On the other hand, ApoB-12a showed the highest turnover ability among AONs tested, but ApoB-12a was shown to be less potent than ApoB-13a *in vivo* (Straarup et al., 2010). Thus, interpreting these data, we must take into account the differences between experimental buffer conditions used here and physiological conditions. For instance, it is known that longer PS-DNAs are more likely to form stronger undesirable complexes with proteins and inactivate RNase H to reduce their efficacy (Gao et al., 1992; Watanabe et al., 2006). As in this system, there are limited accompanying components such as inorganics, proteins, and lipids, and effects including such length-dependent factors may not have been considered. Among the four 10-mer LNAs, ApoB-10a and ApoB-10d showed marked inefficient turnover activity when compared with ApoB-10b and ApoB-10c, indicating a lack of binding affinity. In contrast, the two 20-mer AONs showed inefficient turnover activities when compared with ApoB-20c, probably due to slow product release.

Surprisingly, turnover activities of ApoB-13d and ApoB-13h were exceptionally low, although their *T*m values were in an active range (Fig. 2A). To better understand this observation, we further measured *T*m values of AONs with two additional 10-mer RNAs (MRNA-1, MRNA-2) (Fig. 2B). MRNA-1 and MRNA-2 were prepared as models for the cleaved products of RNase H and correspond to the 5′ and 3′ halves of NL-MRNA, respectively. The results showed that melting temperatures for MRNA-1 were lower than those for MRNA-2, but this trend was reversed in ApoB-13d and ApoB-13h. This potential affinity bias may explain the difference in efficiency of turnover activity. The consensus sequence for the preferred RNase H cleavage sites is unknown; instead, a strong positional preference for cleavage has been observed in a family of enzymes. For example, human RNase H1 has been shown to preferentially cleave the RNA part of RNA/DNA hybrid several nucleotides away from the 5′-RNA/3′-DNA terminus, probably due to the binding directionality of the enzyme (Lima et al., 2007a; Lima et al., 2007b). It has been predicted that the hybrid binding domain of RNase H binds the 5′-RNA/3′-DNA flank of the hybrid relative to the catalytic domain, which is strongly supported by the crystal structure of human RNase H with RNA/DNA hybrids (Nowotny et al., 2007). Despite some reported differences between *E. coli* and human RNase H such as a minimal gap size required for activation of RNase H (Monia et al., 1993; Crooke et al., 1995), the high similarity of the structures of human RNase H1 and *E. coli* RNase H1 suggests that this positional directionality for cleavage encourages ApoB-13d to produce longer RNA segments than fragments

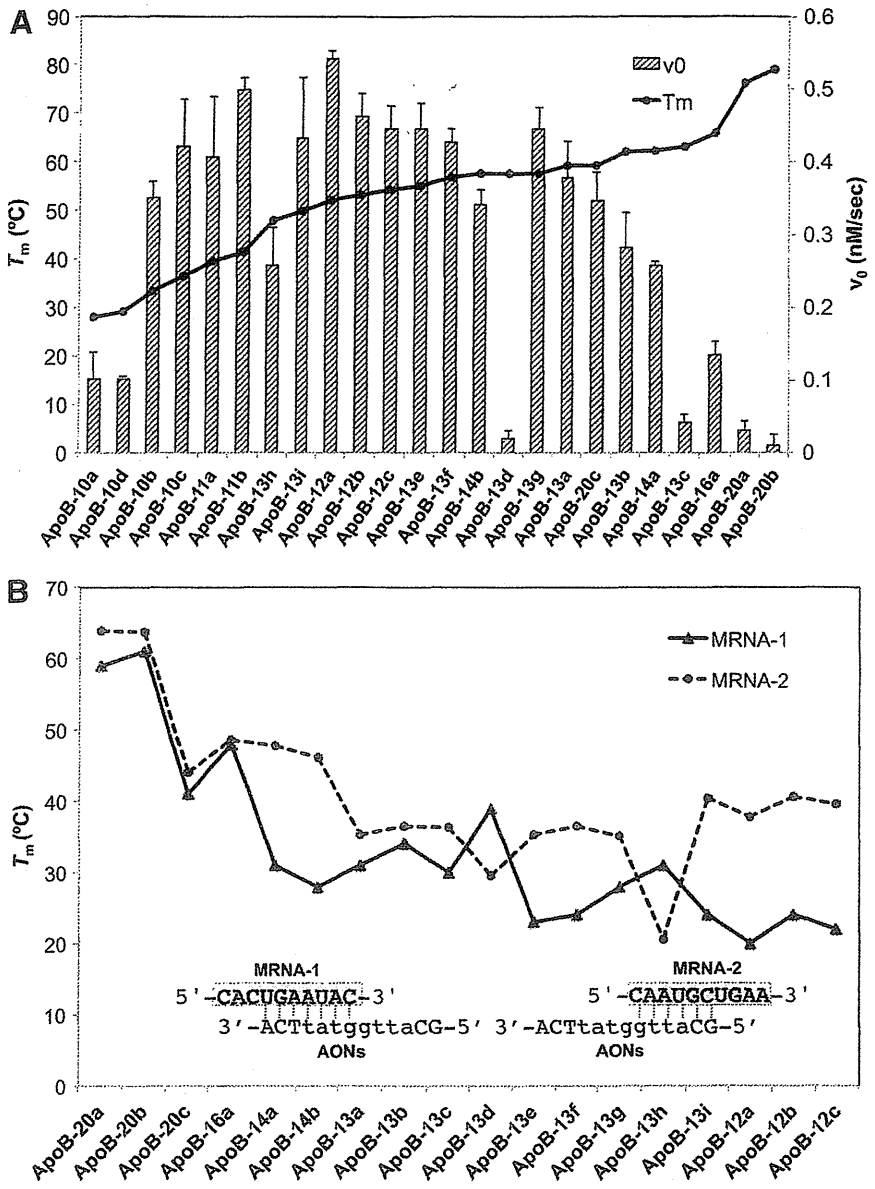

FIG. 2. **(A)** Relationship between turnover rate and gross or local affinity. Initial rates (v_0, bar graph) of turnover reaction rearranged in ascending order of melting temperature (T_m) values (*black line*) of corresponding antisense oligonucleotides (AONs). Data are means ± standard deviation (SD). **(B)** Melting temperatures with MRNA-1 (*solid*) and MRNA-2 (*dotted*). All experiments here were repeated at least three times. Color images available online at www.liebertpub.com/nat

produced by other AONs, thereby forming very stable duplexes with the 3′ half of ApoB-13d and eventually decelerating product release, as well as turnover. Collectively, the requirements for high turnover rates would be adequate binding affinity of the duplex formed by using several bases of AON (for the rapid release of cleaved mRNA), as well as moderate binding affinity of full-length AON/mRNA duplex (for efficient target capture). In contrast, the affinity of the 5′ half of ApoB-13h is thought to be too low to form stable duplexes for cleavage.

In order to explore the capacity of turnover under biological conditions, we attempted to evaluate the *in vivo* efficacy of AONs with identical length (ApoB-13a, -13d, -13e, -13g, and -13h), and to compare the *T*m data relevant to turnover activity. We here adopted a low dosage of 0.75 mg kg^{-1}, which had been confirmed as being sufficient to achieve knockdown of the target apoB mRNA for ApoB-13a, a positive control for *in vivo* screening, because even a single administration of a relatively low dose of 5 mg/kg ApoB-13a had been shown to reduce apoB mRNA by 97%, which made it difficult to discriminate differences in efficacy when AONs screened have similar high efficacy (Straarup et al., 2010). Mice ($n=3$/group) were dosed subcutaneously with 0.75 mg kg^{-1} ApoB-13a, -13d, -13e, -13g and -13h. After 48 hours post-injection, expression levels of apoB mRNA in the liver were analyzed. The apoB mRNA reduction is associated with the clinically relevant therapeutic phenotype characterized by reduced blood cholesterol concentration for the treatment of hypercholesterolemia. Expression levels were rearranged in ascending order of *T*m values of corresponding AONs vs full-length NL-MRNA and are described in Fig. 3. The highest level of reduction in hepatic apoB mRNA was observed in ApoB-13a, while the lowest level of reduction was observed in ApoB-13d and -13h (Fig. 3A; Supplementary Table S3). Statistical significance was seen for ApoB-13a, -13e and -13g, but not for ApoB-13d and -13h. A similar-sized LNA phosphorothioate oligonulecotide without target sites on apoB mRNA was used as a control, showing no decrease in

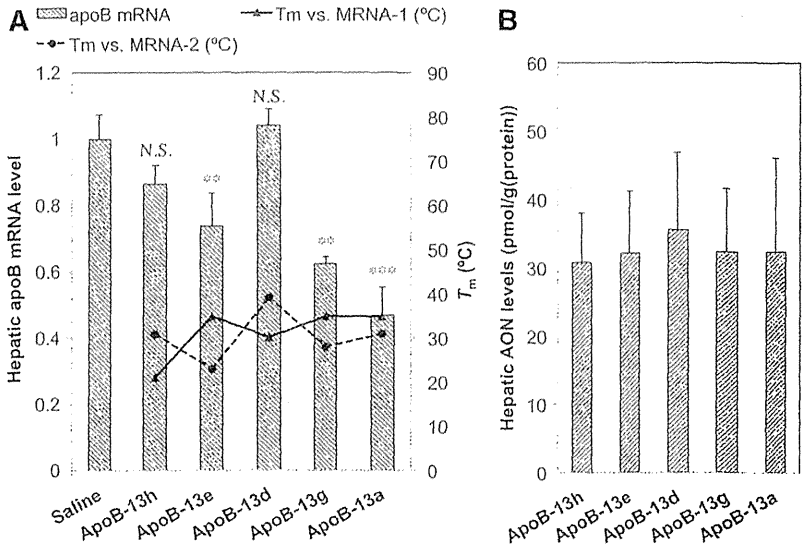

FIG. 3. Reduction of apoB mRNA in the livers (bar graph) of mice ($n=3$/group) receiving a single subcutaneous dose of 0.75 mg kg^{-1} of a series of 13-mer AONs **(A)** rearranged in ascending order of T_m values along with melting temperatures versus MRNA-1 (*solid*) and MRNA-2 (*dashed*). Dunnett's multiple comparison test, $***p<0.001$; $**p<0.01$; N.S., not significant. **(B)** The mouse liver content of a series of 13-mer AONs. Bonferroni multiple comparison tests did not reveal any of arms to be significantly different across groups, $p<0.05$. Error bars represent group means + SD $n=3$.

hepatic apoB mRNA and no potential toxicity (Supplementary Tables S3, S4).

The efficacy order of ApoB-13a > - 13g > - 13e > - 13h > - 13d appears to be unrelated to binding affinity to full-length NL-MRNA, but inefficiency of ApoB-13d and ApoB-13h *in vivo* were consistent with their slow turnover rates in the cell-free system, while other AONs are potent *in vivo* and show fast turnover rates in the cell-free system. Serum reduction levels in total cholesterol denoted the same tendency as mRNA reduction levels (Supplementary Fig. S5). As we selected AONs with an identical length of 13 nt, identical sequences and similar compositions for *in vivo* examination, the mouse liver content of these 13-mer AONs was measured and found to be almost identical (Fig. 3B). In addition to this, we speculate that AONs are not necessarily in vast excess of mRNA even *in vivo*. Sohlenius-Sternbeck has estimated a hepatocellularity number for humans, mice and other animal livers (Sohlenius-Sternbeck, 2006). The value for mice was estimated to be 135×10^6 cells per gram of liver, where livers of 8-week-old mice are 1.0 gram on average. On the other hand, we and others have calculated that approximately <10% of dosed oligonucleotides (<400 pmol for 0.75 mg/kg) reside in liver, even at 48–72 h post-dosing (Straarup et al., 2010; Yamamoto et al., 2012a).

Considering these conditions, each parenchymal cell may be exposed to AONs to a lesser extent than it is in a conventional *in vitro* transfection experiment. Furthermore, nonparenchymal cells such as Kupffer cells are thought to be more likely to ingest AONs than apoB-expressing parenchymal cells do and intracellular distribution of AONs *via* non-productive uptake further reduces the active form of AONs (Koller et al., 2011). In the light of this context, our *in vivo* multiple-turnover hypothesis is a compelling explanation for the *in vivo* activity of AONs. Of course, as there may exist differences such as intracellular distribution of AONs into productive versus less productive compartments, which can be influenced by small changes in chemistry and protein binding ability, it is necessary to continue gathering evidence. This hypothesis may also offer a new direction with regard to the remaining issues in antisense drug development; for example, inconsistency between *in vitro* gene silencing activity of AONs delivered in complex with transfection vehicles and *in vivo* activity of naked AONs (Stein et al., 2010; Zhang et al., 2011).

In the presence of transfection reagents, AONs are delivered quite efficiently to reaction sites, and consequently, might be placed under single-turnover conditions, while inefficient naked conditions may encourage multiple-turnover conditions. However, it should again be noted that it is difficult to monitor the intracellular turnover reaction in living cells and tissues due to their dynamic nature; thus, further experimental support is necessary to determine whether AONs are actually placed under multiple-turnover conditions at the intracellular antisense reaction site. Nevertheless, our study provides an important opportunity to shed light on the uncertain antisense mechanisms, and may lead to further improvement of the activity and safety profiles of AONs.

Acknowledgments

This work was supported by JSPS KAKENHI grant number 24890102 and the Advanced Research for Medical Products Mining Programme of the National Institute of Biomedical Innovation (NIBIO).

Author Disclosure Statement

No competing financial interests exist.

References

CROOKE, S.T., LEMONIDIS, K.M., NEILSON, L., GRIFFEY, R., LESNIK, E.A., and MONIA, B.P. (1995). Kinetic characteristics of Escherichia coli RNase H1: cleavage of various antisense oligonucleotide-RNA duplexes. Biochem. J. **312,** 599–608.

CROOKE, T.S. (2007). Antisense Drug Technologies: Principles, Strategies, and Applications. 2nd ed. (CRC Press Taylor & Francis Group, Boca Raton, FL).

GAO, W.Y., HAN, F.S., STORM, C., EGAN, W., and CHENG, Y.C. (1992). Phosphorothioate oligonucleotides are inhibitors of human DNA polymerases and RNase H: implications for antisense technology. Mol. Pharmacol. **41,** 223–229.

HARI, Y., OBIKA, S., OHNISHI, R., EGUCHI, K., OSAKI, T., OHISHI, H., and IMANISHI, T. (2006). Synthesis and properties of 2′-O,4-C-methyleneoxymethylene bridged nucleic acid. Bioorgan. Med. Chem. **14,** 1029–1038.

HUTVAGNER, G., and ZAMORE, P.D. (2002). A microRNA in a multiple-turnover RNAi enzyme complex. Science **297,** 2056–2060.

KOLLER, E., VINCENT, T. M., CHAPPELL, A., DE, S., MANOHARAN, M., and BENNETT, C. F. (2011). Mechanisms of single-stranded phosphorothioate modified antisense oligonucleotide accumulation in hepatocytes. Nucleic Acids Res. **39,** 4795–4807.

KURRECK, J., WYSZKO, E., GILLEN, C., and ERDMANN, V.A. (2002). Design of antisense oligonucleotides stabilized by locked nucleic acids. Nucleic Acids Res. **30,** 1911–1918.

LIMA, W.F., and CROOKE, S.T. (1997). Binding affinity and specificity of Escherichia coli RNase H1: impact on the kinetics of catalysis of antisense oligonucleotide-RNA hybrids. Biochemistry **36,** 390–398.

LIMA, W.F., ROSE, J.B., NICHOLS, J.G., WU, H.J., MIGAWA, M.T., WYRZYKIEWICZ, T.K., SIWKOWSKI, A.M., and CROOKE, S.T. (2007a). Human RNase H1 discriminates between subtle variations in the structure of the heteroduplex substrate. Mol. Pharmacol. **71,** 83–91.

LIMA, W.F., ROSE, J.B., NICHOLS, J.G., WU, H.J., MIGAWA, M.T., WYRZYKIEWICZ, T.K., VASQUEZ, G., SWAYZE, E.E., and CROOKE, S.T. (2007b). The positional influence of the helical geometry of the heteroduplex substrate on human RNase H1 catalysis. Mol. Pharmacol. **71,** 73–82.

MIYASHITA, K., RAHMAN, S.M.A., SEKI, S., OBIKA, S., and IMANISHI, T. (2007). *N*-Methyl substituted 2′,4′-BNA^{NC}: a highly nuclease-resistant nucleic acid analogue with high-affinity RNA selective hybridization. Chem. Commun. **2007,** 3765–3767.

MONIA, B.P., LESNIK, E.A., GONZALEZ, C., LIMA, W.F., MCGEE, D., GUINOSSO, C.J., KAWASAKI, A.M., COOK, P.D., and FREIER, S.M. (1993). Evaluation of 2′-modified oligonucleotides containing 2′-deoxy gaps as antisense inhibitors of gene expression. J. Biol. Chem. **268,** 14514–14522.

NOWOTNY, M., GAIDAMAKOV, S.A., GHIRLANDO, R., CERRITELLI, S.M., CROUCH, R.J., and YANG, W. (2007). Structure of human RNase h1 complexed with an RNA/DNA hybrid: insight into HIV reverse transcription. Mol. Cell **28,** 264–276.

OBIKA, S., NANBU, D., HARI, Y., ANDOH, J., MORIO, K., DOI, T., and IMANISHI, T. (1998). Stability and structural features of the duplexes containing nucleoside analogues with a fixed N-type conformation, 2′-*O*,4′-*C*-methyleneribonucleosides. Tetrahedron Lett. **39,** 5401–5404.

OBIKA, S., NANBU, D., HARI, Y., MORIO, K., IN, Y., ISHIDA, T., and IMANISHI, T. (1997). Synthesis of 2′-O,4′-C-methyleneuridine and -cytidine. Novel bicyclic nucleosides having a fixed C-3,-endo sugar puckering. Tetrahedron Lett. **38,** 8735–8738.

PRAKASH, T.P., SIWKOWSKI, A., ALLERSON, C.R., MIGAWA, M.T., LEE, S., GAUS, H.J., BLACK, C., SETH, P.P., SWAYZE, E.E., and BHAT, B. (2010). Antisense oligonucleotides containing conformationally constrained 2′,4′-(N-methoxy)aminomethylene and 2′,4′-aminooxymethylene and 2′-O,4′-C-aminomethylene bridged nucleoside analogues show improved potency in animal models. J. Med. Chem. **53,** 1636–1650.

SETH, P.P., SIWKOWSKI, A., ALLERSON, C.R., VASQUEZ, G., LEE, S., PRAKASH, T.P., WANCEWICZ, E.V., WITCHELL, D., and SWAYZE, E.E. (2009). Short antisense oligonucleotides with novel 2′-4′ conformationaly restricted nucleoside analogues show improved potency without increased toxicity in animals. J. Med. Chem. **52,** 10–13.

SINGH, S.K., NIELSEN, P., KOSHKIN, A.A., and WENGEL, J. (1998). LNA (locked nucleic acids): synthesis and high-affinity nucleic acid recognition. Chem. Commun. **1998,** 455–456.

SOHLENIUS-STERNBECK, A.K. (2006) Determination of the hepatocellularity number for human, dog, rabbit, rat and mouse livers from protein concentration measurements. Toxicol. In Vitro **20,** 1582–1586.

STANTON, R., SCIABOLA, S., SALATTO, C., WENG, Y., MOSHINSKY, D., LITTLE, J., WALTERS, E., KREEGER, J., et al. (2012). Chemical modification study of antisense gapmers. Nucleic Acid Ther. **22,** 344–359.

STEIN, C.A., HANSEN, J.B., LAI, J., WU, S., VOSKRESENSKIY, A., HOG, A., WORM, J., HEDTJARN, M., SOULEIMANIAN, N., MILLER, P., et al. (2010). Efficient gene silencing by delivery of locked nucleic acid antisense oligonucleotides, unassisted by transfection reagents. Nucleic Acids Res. **38,** e3.

STRAARUP, E.M., FISKER, N., HEDTJARN, M., LINDHOLM, M.W., ROSENBOHM, C., AARUP, V., HANSEN, H.F., ORUM, H., HANSEN, J.B., and KOCH, T. (2010). Short locked nucleic acid antisense oligonucleotides potently reduce apolipoprotein B mRNA and serum cholesterol in mice and non-human primates. Nucleic Acids Res. **38,** 7100–7111.

VESTER, B., BOEL, A.M., LOBEDANZ, S., BABU, B.R., RAUNKJAER, M., LINDEGAARD, D., RAUNAK, HRDLICKA, P.J., HOJLAND, T., et al. (2008). Chemically modified oligonucleotides with efficient RNase H response. Bioorg. Med. Chem. Lett. **18,** 2296–2300.

WATANABE, T.A., GEARY, R.S., and LEVIN, A.A. (2006). Plasma protein binding of an antisense oligonucleotide targeting human ICAM-1 (ISIS 2302). Oligonucleotides **16,** 169–180.

YAHARA, A., SHRESTHA, A.R., YAMAMOTO, T., HARI, Y., OSAWA, T., YAMAGUCHI, M., NISHIDA, M., KODAMA, T., and OBIKA, S. (2012). Amido-bridged nucleic acids (AmNAs): synthesis, duplex stability, nuclease resistance, and in vitro antisense potency. Chembiochem **13,** 2513–2516.

YAMAMOTO, T., HARADA-SHIBA, M., NAKATANI, M., WADA, S., YASUHARA, H., NARUKAWA, K., SASAKI, K., SHIBATA, M.A., TORIGOE, H., et al. (2012a). Cholesterol-lowering action of BNA-based antisense oligonucleotides targeting PCSK9 in atherogenic diet-induced hypercholesterolemic mice. Mol. Ther. Nucleic Acids **1,** e22.

YAMAMOTO, T., NAKATANI, M., NARUKAWA, K., and OBIKA, S. (2011). Antisense drug discovery and development. Future Med. Chem. **3,** 339–365.

YAMAMOTO, T., YASUHARA, H., WADA, F., HARADA-SHIBA, M., IMANISHI, T., and OBIKA, S. (2012b). Superior silencing by 22,42-BNA^{NG}-Based short antisense oligonucleotides compared to 22,42-BNA/LNA-based apolipoprotein B antisense inhibitors. J. Nucleic Acids, Article ID 707323.

ZHANG, Y., QU, Z., KIM, S., SHI, V., LIAO, B., KRAFT, P., BANDARU, R., WU, Y., GREENBERGER, L.M., and HORAK, I.D. (2011). Down-modulation of cancer targets using locked nucleic acid (LNA)-based antisense oligonucleotides without transfection. Gene Ther, **18,** 326–333.

Address correspondence to:
Satoshi Obika, PhD
Graduate School of Pharmaceutical Sciences
Osaka University
1-6 Yamadaoka
Suita, Osaka 565-0871
Japan

E-mail: obika@phs.osaka-u.ac.jp

Received for publication October 23, 2013; accepted after revision March 13, 2014.

Jpn J Radiol (2014) 32:80–89
DOI 10.1007/s11604-013-0272-y

ORIGINAL ARTICLE

Apparent diffusion coefficient is a prognostic factor of head and neck squamous cell carcinoma treated with radiotherapy

Masamitsu Hatakenaka · Katsumasa Nakamura · Hidetake Yabuuchi · Yoshiyuki Shioyama · Yoshio Matsuo · Takeshi Kamitani · Masato Yonezawa · Takashi Yoshiura · Torahiko Nakashima · Mitsuru Mori · Hiroshi Honda

Received: 29 October 2013 / Accepted: 9 December 2013 / Published online: 10 January 2014
© Japan Radiological Society 2014

Abstract
Purpose To evaluate the correlation between apparent diffusion coefficient (ADC) and prognosis in head and neck squamous cell carcinoma (HNSCC) treated with radiotherapy.
Materials and methods We retrospectively studied 41 patients (38 male and 3 female, ages 37–85 years) diagnosed with HNSCC (14 oropharynx, 22 hypopharynx, 4 larynx, 1 oral cavity) and treated with radiotherapy, with radiation dose to gross tumor volume over 60 Gy. The association between age, gender, performance status, tumor location, *T* stage, *N* stage, stage, dose, overall treatment time, treatment method, adjuvant therapy, or ADC and prognosis was analyzed using a Cox proportional hazard test.
Results ADC calculated with *b*-values of 300, 500, 750, and 1,000 s/mm^2 (ADC 300–1,000) alone showed a significant correlation with all of the analyses ($p = 0.022$ for local control, $p = 0.0109$ for regional control, $p = 0.0041$ for disease-free survival, and $p = 0.0014$ for overall survival). ADC calculated with *b*-values of 0, 100, and 200 s/mm^2 (ADC 0–200) showed a significant correlation with overall survival ($p = 0.0012$). *N* stage showed a significant correlation with regional control ($p = 0.0241$). Performance status showed significant association with local control ($p = 0.0459$), disease-free survival ($p = 0.023$), and overall survival ($p = 0.0151$), respectively.
Conclusion ADC is an independent predictor of prognosis in HNSCC treated with radiotherapy.

Keywords Apparent diffusion coefficient · Bystander effect · Head and neck cancer · Prognosis · Radiotherapy

M. Hatakenaka (✉)
Department of Diagnostic Radiology, School of Medicine, Sapporo Medical University, Minami 1, Nishi 17, Chuo-ku, Sapporo 060-8556, Japan
e-mail: mhatakenaka@sapmed.ac.jp

K. Nakamura · Y. Matsuo · T. Kamitani · M. Yonezawa · T. Yoshiura · H. Honda
Department of Clinical Radiology, Graduate School of Medical Sciences, Kyushu University, Fukuoka, Japan

H. Yabuuchi
Department of Health Sciences, Graduate School of Medical Sciences, Kyushu University, Fukuoka, Japan

Y. Shioyama
Department of Heavy Particle Therapy and Radiation Oncology, Graduate School of Medical Sciences, Kyushu University, Fukuoka, Japan

T. Nakashima
Department of Otorhinolaryngology, Graduate School of Medical Sciences, Kyushu University, Fukuoka, Japan

M. Mori
Department of Public Health, School of Medicine, Sapporo Medical University, Minami 1, Nishi 17, Chuo-ku, Sapporo, Japan

Introduction

Head and neck squamous cell carcinoma (HNSCC) is the fifth most common neoplasm worldwide [1], and approximately two-thirds of HNSCC patients present with advanced-stage disease, commonly involving regional nodes. However, distant metastasis at the initial presentation is not common (approximately one-tenth of all patients) [2]. Among treatment options, chemoradiotherapy is increasingly being chosen as an organ-sparing primary treatment.

The self-diffusion of cell water is theoretically affected by temperature and viscosity, but it is also affected by

barrier structures such as cell membranes, because it takes some time to measure proton diffusion with magnetic resonance (MR) imaging [3]. Diffusion-weighted (DW) MR imaging thus provides microstructural information about tissues [4]. Several studies have used apparent diffusion coefficient (ADC) as an indicator for treatment response, revealing that pretreatment ADC correlates with treatment response [5–8] and that changes or the absence of changes in ADC at an early phase of treatment can predict treatment response [9–13].

Although chemoradiotherapy is increasingly being chosen as a primary treatment option for HNSCC, there have been few studies applying ADC as a prognostic factor [14–21]. To the best of our knowledge, few clinical studies have ever evaluated the usefulness of ADC as an indicator for disease-free or overall survival using multivariate analysis. We hypothesized that pretreatment ADC would correlate not only with local control but also with regional control, disease-free survival, and overall survival in HNSCC treated with radiotherapy.

Materials and methods

This study was approved by the Committee on Clinical Study at our institute. Informed consent was waived for the retrospective study. The patients analyzed in the present study overlapped with those of previous studies [17, 18, 21]. However, the present study analyzed not only local control but also regional control as well as disease-free and overall survival while the previous studies analyzed local control alone.

Patients

We enrolled 62 consecutive patients, who were histologically proved to have primary HNSCC, at our institute between April 2006 and August 2009. These were scheduled to receive radical radiotherapy [>60 Gy to gross tumor volume (GTV)] and underwent MR imaging, including DW imaging, before treatment. Among the 62 patients enrolled, 8 patients with diagnoses of nasopharyngeal cancer were excluded because nasopharyngeal cancer is known to be more radiosensitive than other types of HNSCC. Seven patients were excluded because detection and/or demarcation of the primary lesion on DW imaging was difficult due to small lesions or artifacts, and 6 patients were excluded because the radiation dose to the GTV was <60 Gy due to poor patient conditions or severe side effects. Therefore, we studied 41 patients (14 oropharynx, 22 hypopharynx, 4 larynx, 1 oral cavity; all squamous cell carcinoma) who received radiotherapy with

Table 1 Characteristics of the patients, diseases, and treatments

Variable	Case
Age (years)	
Range	37–85
Median	64
Gender	
Male	38
Female	3
Performance status	
0	24
1	10
2	6
3	1
Tumor location	
Oropharynx	14
Hypopharynx	22
Larynx	4
Oral cavity	1
T stage	
1	2
2	22
3	8
4	9
N stage	
0	8
1	6
2	21
3	6
M stage	
0	41
Stage	
1	1
2	7
3	6
4	27
Dose (Gy)	
Range	64–71
Median	65.4
OTT (days)	
Range	43–91
Median	63
Treatment method	
Radiotherapy alone	5
Chemoradiotherapy using TS-1	33
Chemoradiotherapy using CDDP	3
Adjuvant chemotherapy	
Positive	21
Negative	20
ADC 0–200 (10^{-3} mm^2/s)	
Range	0.78–3.30

Table 1 continued

Variable	Case
Mean	1.67
ADC 300–1,000 (10^{-3} mm^2/s)	
Range	0.40–1.35
Mean	0.81

a radiation dose to GTV over 60 Gy (64–71 Gy, median 65.4 Gy) and had MR imaging before treatment, including DW imaging. TNM stages were classified according to the International Union Against Cancer staging system 2002. No patients had a history of receiving chemotherapy or radiotherapy. The patient, disease, and treatment characteristics are summarized in Table 1.

Treatment and follow-up

External radiotherapy was performed with 4- or 6-MV X-ray in 1.8–2.0 Gy fractions at 5 fractions per week using a three-dimensional conformal technique. Concurrent chemoradiotherapy was administered to 36 patients [TS-1 for 33 patients: 65 mg/m^2 for 4 weeks followed by 2 weeks of rest while receiving radiotherapy; cisplatin (CDDP) for 3 patients: 5 mg/m^2 for 5 days a week while receiving radiotherapy] and the remaining 5 patients were treated with radiotherapy alone due to their condition.

The patients were followed up for the evaluation of local and regional control and for distant metastasis. The follow-up evaluations included physical, endoscopic, and radiological examinations. Contrast-enhanced computed tomography (CT) was the base of the radiological examination, and MR imaging and/or (18)F-fluorodeoxyglucose positron emission tomography (PET)/CT images were obtained when the otorhinolaryngologists considered these examinations necessary. Histologically confirmed local and/or regional recurrences during follow-up were considered local and/or regional failures, respectively. Distant metastasis was defined as a newly appearing lesion that increased in size on follow-up imaging exams with reference to (18)F-fluorodeoxyglucose PET/CT when needed.

The follow-up period was designated as the total time of follow-up starting at treatment initiation. Regarding local and regional control, the follow-up period ended either at histologically confirmed local and/or regional failure or at the last patient contact without local or regional failure. For disease-free survival, it ended at local or regional failure, distant metastasis, or the last patient contact without local or regional failure, or distant metastasis. For overall survival, it ended either at patient death or the last patient contact.

MR imaging

MR imaging was performed using a 1.5-T system (Intera Achieva; Philips Medical Systems, Best, the Netherlands) before the initiation of treatment. The field of view was 200–230 mm with a slice thickness of 3–5 mm, and a neurovascular coil with sensitivity encoding was used. Pretreatment images were obtained at a median of 8 days (range 0–26 days) before the start of radiotherapy.

T2-weighted turbo spin-echo, T1-weighted, DW, and gadolinium-enhanced T1-weighted transverse images of the neck were obtained at pretreatment imaging, and coronal and/or sagittal images were also obtained when needed. The imaging parameters for DW imaging were as follows: matrix 256 × 112; repetition time 3,000 ms; echo time 73 ms; *b*-factors 0, 100, 200, 300, 500, 750 and 1,000 s/mm^2; number of excitations 2; examination duration 4 min 6 s. DW imaging was obtained with a

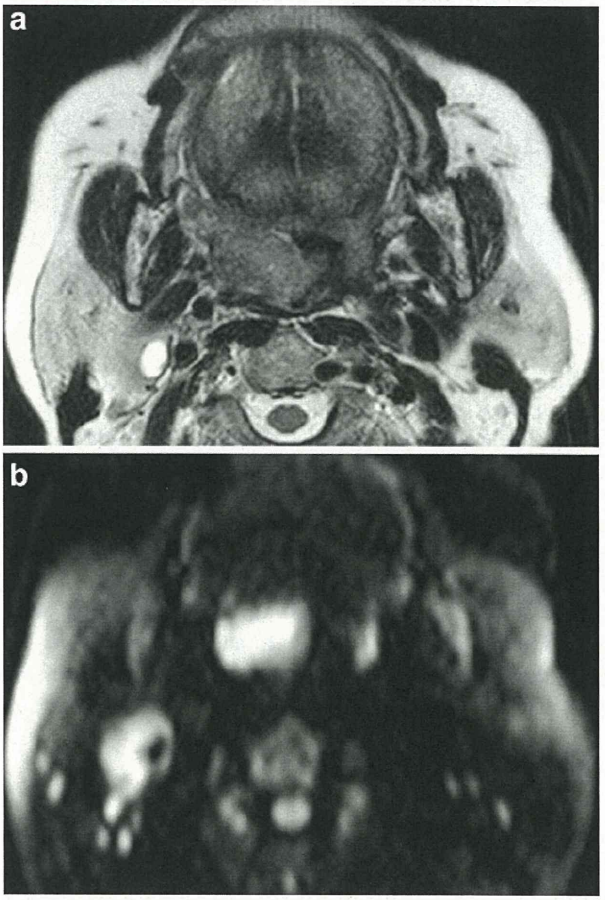

Fig. 1 A representative good-prognosis woman in her 70s (disease-free survival with 36.8 months follow-up) with oropharyngeal cancer (T2N2M0, performance status 0, ADC 0–200 = 2.18 × 10^{-3} mm^2/s, ADC 300–1,000 = 0.57 × 10^{-3} mm^2/s). **a** T2-weighted transverse image. **b** DW transverse image (b = 1,000 s/mm^2)

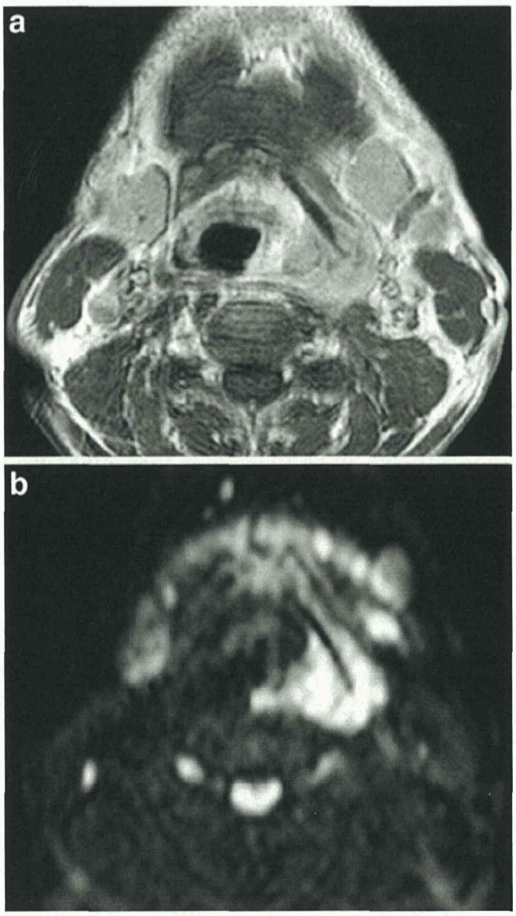

Fig. 2 A representative poor-prognosis man in his 50s (local and regional failure at 3.3 months follow-up and died at 13.1 months follow-up) with hypopharyngeal cancer (T4N2M0, performance status 0, ADC 0–200 = 1.65×10^{-3} mm^2/s, ADC 300–1,000 = 0.90×10^{-3} mm^2/s). **a** Gadolinium-enhanced T1-weighted transverse image. **b** DW transverse image (b = 1,000 s/mm^2)

single-shot spin-echo echo-planar imaging sequence using a spectral presaturation with inversion recovery for fat suppression. The motion-probing gradient pulses were placed along the x-, y-, and z-axes and synthesized images from the 3 images were used. Representative images are shown in Figs. 1 and 2.

ADC calculation

The region of interest (ROI) was designated as the primary lesion at the level of the largest tumor diameter on DW images of each b-value to cover most of the lesion, while avoiding cystic or necrotic components with reference to conventional MR images. This procedure was independently performed by two of the authors (board-certified diagnostic radiologists with 17 and 8 years of experience, respectively) without information regarding prognosis. The ADC was calculated as follows: the mean signal intensities (SIs) of the ROI under various b-values were fitted to the equation $SI = SI_0e^{-bD}$, where SI is the measured signal intensity, SI_0 is the SI at b-value 0, b is the strength of the motion-probing gradient, and D stands for ADC. An ADC calculated with b-values of 0, 100, and 200 s/mm^2 was taken as the value of ADC 0–200, and ADC calculated with b-values of 300, 500, 750, and 1,000 s/mm^2 as ADC 300–1,000, respectively. The mean ADC 0–200 and ADC 300–1,000 values obtained by the two radiologists were considered the ADC 0–200 and ADC 300–1,000 values for each lesion, respectively.

Statistics

The variables [age, gender, performance status (PS01 vs PS23), tumor location (hypopharynx vs others), T stage (T12 vs T34), N stage (N01 vs N23), stage (123 vs 4), dose, overall treatment time (OTT), treatment method (chemoradiotherapy vs radiotherapy alone), adjuvant chemotherapy (positive vs negative)], ADC 0–200, and ADC 300–1,000 were selected and tested for their correlation with local failure, regional failure, disease-free survival, and overall survival. To identify an optimal threshold for a binary classifier, a receiver operating characteristic curve analysis was performed for numerical data.

In the univariate survival analysis, the curves for local control, regional control, disease-free survival, and overall survival were estimated using the Kaplan–Meier method, and the log rank test was used to test the differences. The variables showing significant correlation in a log rank test were further tested by multivariate survival analysis using a Cox proportional hazard test. The correlation of ADC between the two radiologists was analyzed by calculating the interclass correlation coefficient (ICC).

The statistical calculations were performed in consultation with a biostatistician using statistical analysis software (JMP, version 7.0.1, SAS, Cary, NC, USA; Prism, version 5.02, GraphPad, San Diego, CA, USA; and SPSS, version 16, SPSS, Chicago, IL, USA). Values of $p < 0.05$ were considered significant.

Results

Prognosis

Twelve patients developed local failure (follow-up time 2.0–17.5 months with a median of 3.8 months) and the remaining 29 showed local control (follow-up time 5.3–54.8 months with a median of 35.5 months). Twelve patients developed regional failure (follow-up time

Table 2 Correlation of each variable with local control

Variable	*p* value	
	Log rank test	Cox proportional hazard test
Age (years)		
≥75 vs <75	NS	
Gender		
Male vs female	NS	
Performance status		
PS 01 vs PS 23	**<0.0001**	**0.0459**
Tumor location		
Hypopharynx vs others	NS	
***T* stage**		
T 12 vs T 34	**0.0003**	NS
N stage		
N 01 vs N 23	NS	
Stage		
Stage 123 vs stage 4	NS	
Dose (Gy)		
≥66 vs <66	NS	
OTT (days)		
≥55 vs <55	NS	
Treatment method		
Chemoradiotherapy vs radiotherapy alone	**0.0005**	NS
Adjuvant chemotherapy		
Positive vs negative	NS	
ADC 0–200 (10^{-3} mm^2/s)		
≥1.85 vs <1.85	**0.0298**	NS
ADC 300–1,000 (10^{-3} mm^2/s)		
≥0.86 vs <0.86	**<0.0001**	**0.0220**

Variables in bold face mean $p < 0.05$

NS means $p > 0.05$

Table 3 Correlation of each variable with regional control

Variable	*p* value	
	Log rank test	Cox proportional hazard test
Age (years)		
≥71 vs <71	NS	
Gender		
Male vs female	NS	
Performance status		
PS 01 vs PS 23	**0.0153**	NS
Tumor location		
Hypopharynx vs others	NS	
T stage		
T 12 vs T 34	NS	
***N* stage**		
N 01 vs N 23	**0.0336**	**0.0241**
Stage		
Stage 123 vs stage 4	**0.0336**	–
Dose (Gy)		
≥66 vs <66	NS	
OTT (days)		
≥60 vs <60	NS	
Treatment method		
Chemoradiotherapy vs radiotherapy alone	NS	
Adjuvant chemotherapy		
Positive vs negative	NS	
ADC 0–200 (10^{-3} mm^2/s)		
≥1.80 vs <1.80	NS	
ADC 300–1,000 (10^{-3} mm^2/s)		
≥0.70 vs <0.70	**0.027**	**0.0109**

Stage was not applied for multivariate analysis because there was a significant correlation between *N* stage and stage

Variables in bold face mean $p < 0.05$

NS means $p > 0.05$

2.0–9.3 months with a median of 3.5 months) and the remaining 29 showed regional control (follow-up time 6.1–54.8 months with a median of 35.0 months). Seven patients developed both local and regional failure. Twenty-one patients developed disease recurrence or metastasis (follow-up time 2.0–27.4 months with a median of 3.9 months) and the remaining 20 showed disease-free survival (follow-up time 11.3–54.8 months with a median of 36.8 months). Eleven patients died (follow-up time 2.1–27.0 months with a median of 10.5 months) and the remaining 30 survived (follow-up time 5.3–54.8 months with a median of 35.9 months).

Survival analyses

Regarding local control, the variables of performance status (0,1 vs 2,3), *T* stage (12 vs 34), treatment method (chemoradiotherapy vs radiotherapy alone), ADC 0–200 (≥1.85 vs <1.85 × 10^{-3} mm^2/s), and ADC 300–1,000 (≥0.86 vs <0.86 × 10^{-3} mm^2/s) showed significance in the univariate survival analysis using a log rank test. Performance status (01 vs 23) and ADC 300–1,000 (≥0.86 vs <0.86 × 10^{-3} mm^2/s) showed significance in multivariate analysis using a Cox proportional hazard test (Table 2). Regarding regional control, performance status (01 vs 23), *N* stage (01 vs 23), stage (123 vs 4), and ADC 300–1,000 (≥0.70 vs <0.70 × 10^{-3} mm^2/s) showed significance in a log rank test. *N* stage (01 vs 23) and ADC 300–1,000 (≥0.70 vs <0.70 × 10^{-3} mm^2/s) showed significance in a Cox proportional hazard test (Table 3). Stage was removed from multivariate analysis because there was a significant correlation between *N* stage and stage ($p < 0.01$,

Table 4 Correlation of each variable with disease-free survival

Variable	*p* value	
	Log rank test	Cox proportional hazard test
Age (years)		
≥63 vs <63	NS	
Gender		
Male vs female	NS	
Performance status		
PS 01 vs PS 23	**<0.0001**	**0.023**
Tumor location		
Hypopharynx vs others	NS	
***T* stage**		
T 12 vs T 34	**0.0461**	NS
N stage		
N 01 vs N 23	NS	
Stage		
Stage 123 vs stage 4	NS	
Dose (Gy)		
≥66 vs <66	NS	
OTT (days)		
≥66 vs <66	NS	
Treatment method		
Chemoradiotherapy vs radiotherapy alone	**0.003**	NS
Adjuvant chemotherapy		
Positive vs negative	NS	
ADC 0–200 (10^{-3} mm^2/s)		
≥1.80 vs <1.80	NS	
ADC 300–1,000 (10^{-3} mm^2/s)		
≥0.725 vs <0.725	**0.0004**	**0.0041**

Variables in bold face mean $p < 0.05$

NS means $p > 0.05$

Table 5 Correlation of each variable with overall survival

Variable	*p* value	
	Log rank test	Cox proportional hazard test
Age (years)		
≥76 vs <76	NS	
Gender		
Male vs female	NS	
Performance status		
PS 01 vs PS 23	**0.0001**	**0.0151**
Tumor location		
Hypopharynx vs others	NS	
***T* stage**		
T 12 vs T 34	**0.0131**	NS
N stage		
N 01 vs N 23	NS	
Stage		
Stage 123 vs stage 4	NS	
Dose (Gy)		
≥66 vs <66	**0.0414**	NS
OTT (days)		
≥65 vs <65	NS	
Treatment method		
Chemoradiotherapy vs radiotherapy alone	NS	
Adjuvant chemotherapy		
Positive vs negative	NS	
ADC 0–200 (10^{-3} mm^2/s)		
≥1.85 vs <1.85	**0.0092**	**0.0012**
ADC 300–1,000 (10^{-3} mm^2/s)		
≥0.84 vs <0.84	**0.0004**	**0.0014**

Variables in bold face mean $p < 0.05$

NS means $p > 0.05$

Spearman's rank correlation coefficient). Performance status (01 vs 23), *T* stage (12 vs 34), treatment method (chemoradiotherapy vs radiotherapy alone), and ADC 300–1,000 (≥0.725 vs <0.725 × 10^{-3} mm^2/s) showed significance on disease-free survival using a log rank test. Performance status (01 vs 23) and ADC 300–1,000 (≥0.725 vs <0.725 × 10^{-3} mm^2/s) showed significance in a multivariate analysis using a Cox proportional hazard test (Table 4). Regarding overall survival, performance status (01 vs 23), *T* stage (12 vs 34), dose (≥66 vs <66 Gy), ADC 0–200 (≥1.85 vs <1.85 × 10^{-3} mm^2/s), and ADC 300–1,000 (≥0.84 vs <0.84 × 10^{-3} mm^2/s) showed significance in a log rank test. Performance status (01 vs 23), ADC 0–200 (≥1.85 vs <1.85 × 10^{-3} mm^2/s), and ADC 300–1,000 (≥0.84 vs <0.84 × 10^{-3} mm^2/s) showed significance in a Cox proportional hazard test (Table 5). The survival curve results are summarized in Fig. 3.

Correlation of ADC between radiologists

The ICCs for ADC 0–200 and ADC 300–1,000 were 0.826 (95 % confidence interval 0.697–0.903) and 0.715 (95 % confidence interval 0.525–0.837), respectively.

Fig. 3 Survival curves. **a** Comparison of local control curves between ADC 300–1,000 ≥ 0.86 × 10^{-3} and <0.86 × 10^{-3} mm^2/s. **b** Comparison of local control curves between ADC 0–200 ≥ 1.85 × 10^{-3} and <1.85 × 10^{-3} mm^2/s. **c** Comparison of regional control curves between ADC 300–1,000 ≥ 0.70 × 10^{-3} and <0.70 × 10^{-3} mm^2/s. **d** Comparison of disease-free survival curves between ADC 300–1,000 ≥ 0.725 × 10^{-3} and <0.725 × 10^{-3} mm^2/s. **e** Comparison of overall survival curves between ADC 300–1,000 ≥ 0.84 × 10^{-3} and <0.84 × 10^{-3} mm^2/s. **f** Comparison of overall survival curves between ADC 0–200 ≥ 1.85 × 10^{-3} and <1.85 × 10^{-3} mm^2/s

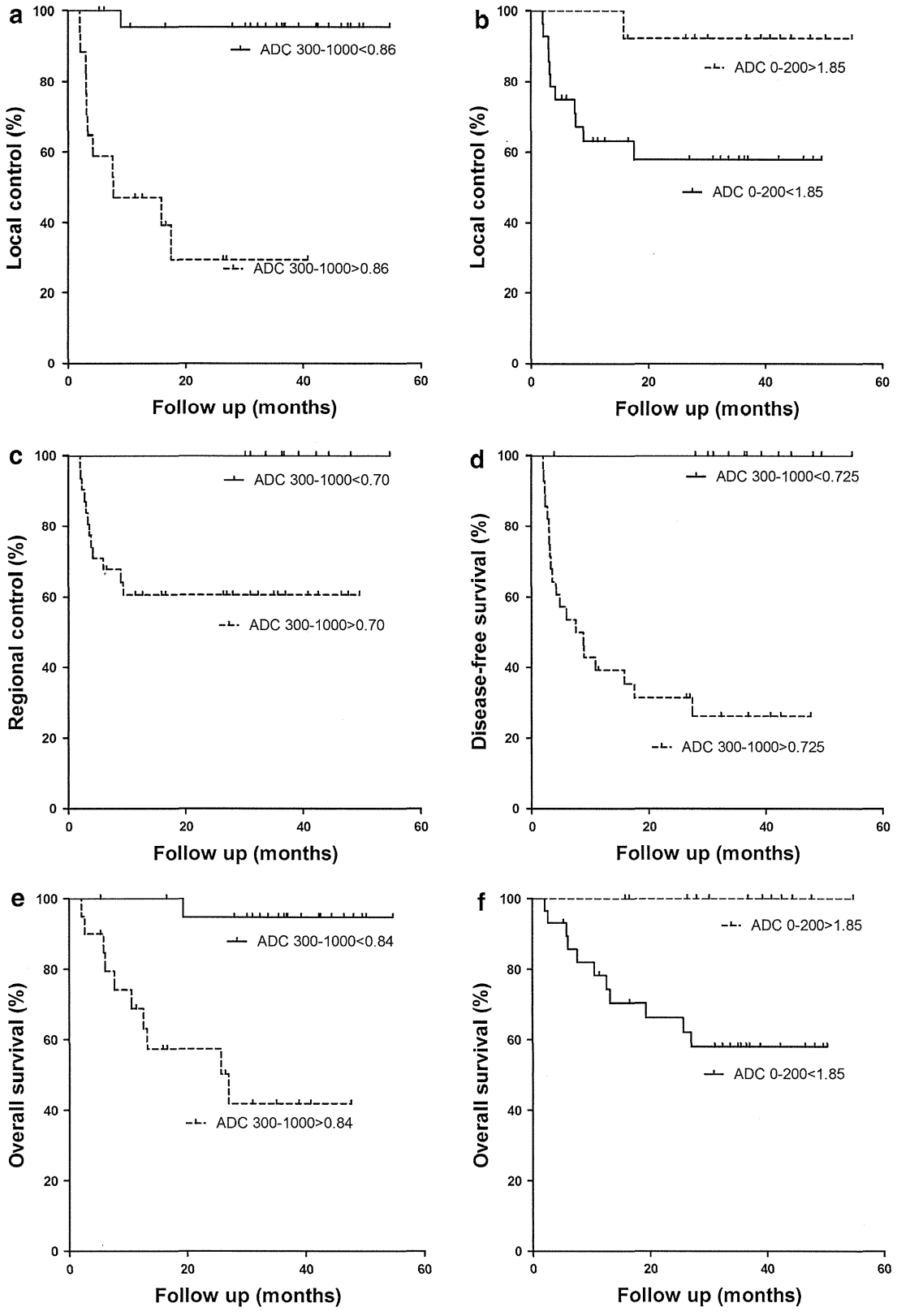
a
Local control (%)
ADC 300-1000<0.86
ADC 300-1000>0.86
Follow up (months)
b
Local control (%)
ADC 0-200>1.85
ADC 0-200<1.85
Follow up (months)
c
Regional control (%)
ADC 300-1000<0.70
ADC 300-1000>0.70
Follow up (months)
d
Disease-free survival (%)
ADC 300-1000<0.725
ADC 300-1000>0.725
Follow up (months)
e
Overall survival (%)
ADC 300-1000<0.84
ADC 300-1000>0.84
Follow up (months)
f
Overall survival (%)
ADC 0-200>1.85
ADC 0-200<1.85
Follow up (months)

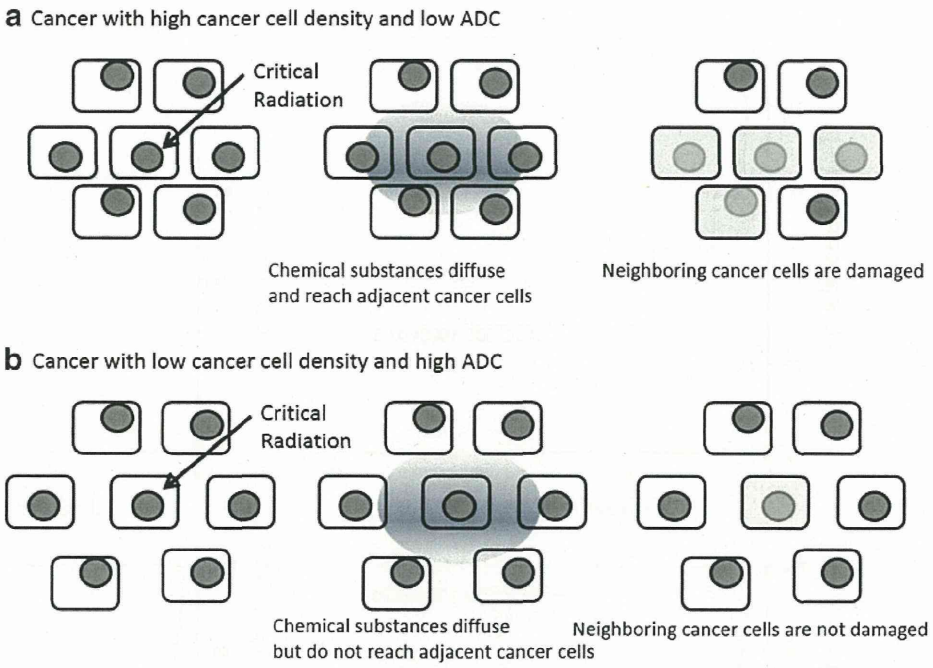

Fig. 4 Proposed mechanism of the correlation between ADC and radiosensitivity. **a** Cancer with high cancer cell density and low ADC. The chemical substances released from heavily damaged cancer cells diffuse, reach adjacent cancer cells, and affect them, resulting in a radiosensitive cancer. **b** Cancer with low cancer cell density and high ADC. The chemical substances released from heavily damaged cancer cells diffuse but do not reach or affect adjacent cancer cells, resulting in a radioresistant cancer

Discussion

The results of the present study show that ADC calculated from DW imaging is a predictor of prognosis in HNSCC treated with radiotherapy. ADC 300–1,000 calculated with relatively high *b*-values is an independent predictor of prognosis (local and regional control, and disease-free and overall survival). ADC 0–200 calculated with relatively low *b*-values is also a predictor of overall survival.

There have been some studies evaluating the relation between ADC and treatment response or prognosis in HNSCC treated with radiotherapy. However, their results have differed. The present results are in accordance with the previous reports that lower pretreatment ADC correlates with good treatment response [14, 15], local control [17, 18, 21], and prognosis [20]. In contrast, there have been studies reporting that pretreatment ADC does not correlate with local or regional control but ADC change values 3 weeks after the initiation of treatment or the ADC change ratio 3 weeks after the completion of treatment correlate with local or regional control in HNSCC treated with radiotherapy [16, 19]. The reasons for these different results were unclear. The present study was designed to shed some light onto this problem, and a possible reason for these differences is as follows. As shown in Tables 2 and 5, and Fig. 3, a higher ADC 0–200 showed a favorable prognosis in contrast with ADC 300–1,000, which showed the opposite directional correlation with prognosis, which was that of lower ADC 300–1,000 with favorable prognosis. When ADC is calculated with both relatively low and high *b*-values, it is thought to include these opposite characteristics. This might be the reason that ADC calculated with both relatively low and high *b*-values, e.g. 0 and 1,000 s/mm^2, is not significantly correlated with prognosis. It was reported that ADC calculated with *b*-values of 0 and 1,000 s/mm^2 is not significantly correlated with overall survival in HNSCC treated with radiotherapy, which would support our interpretation [22]. We consider that DW imaging with several *b*-values would be preferable for predicting the prognosis. In contrast, a lower minimum ADC was reported to be an unfavorable prognostic factor for distant metastasis-free and overall survival in malignant mucosal melanoma treated with carbon ion radiotherapy and concurrent chemotherapy. The difference in ADC calculating method, in which the authors also calculated ADC with relatively low and high *b*-values, and the difference in histology and treatment method might have affected the results [8].

The mechanisms underlying the correlation between pretreatment ADC and prognosis are unclear. We propose a possible theory as follows: cancers with low ADC usually show high cell density [23]. The spatial distribution of photons is usually not homogeneous for each cancer cell, and this causes critical damage to some cancer cells but is not critical for adjacent other cancer cells. When one cancer cell undergoes critical damage, it could release chemical substances, and these substances diffuse and can reach adjacent cancer cells; this process could increase the damage level to the cancer cells from sub-lethal to lethal, resulting in increasing radiation sensitivity. In contrast, in cancers with high ADC and low cancer cell density, the chemical substances released from critically damaged

cancer cells would also diffuse but would not reach neighboring cancer cells at effective concentrations (because the distances between cancer cells are greater), thus causing no critical damage to the neighboring cancer cells, resulting in radiation resistance. These mechanisms are summarized in Fig. 4. This theory is supported by the findings that cells exposed to radiation can release signals that induce similar effects in non-targeted neighboring cells (bystander effect). These irradiated cells secrete cytokines or other factors [e.g. reactive oxygen species, interleukin 8, transforming growth factor β, soluble death ligands Fas, tumor necrosis factor-related apoptosis-inducing ligand, and tumor necrosis factor α] that induce an increased intracellular level of reactive oxygen species in unirradiated cells [24].

Regarding mechanisms of the correlation between ADC 0–200 and prognosis, ADC calculated with relatively low *b*-values is thought to correlate with perfusion [25, 26] and tumors with high perfusion are known to be oxygen-rich and radiosensitive. As a result, a tumor with high perfusion probably shows high ADC 0–200 and favorable prognosis (Tables 2, 5; Fig. 3).

The demarcations of lesions can differ among radiologists, and this difference could affect the results. However, the results obtained here by two independent radiologists showed excellent and good correlations in ADC 0–200 and ADC 300–1,000, respectively, according to the following criteria (ICC <0.4, poor; $0.4 \leq$ ICC ≤ 0.59, fair; $0.6 \leq$ ICC ≤ 0.74, good; ICC ≥ 0.75, excellent) [27]. Thus, we believe that our method was robust and reliable.

The present result that performance status correlated with local control, disease-free and overall survival is consistent with previous knowledge. Performance status has been known to be a robust prognostic factor irrespective of cancer histology or treatment method. The result that *N* stage correlated with regional control is also consistent with previous knowledge. However, *N* stage was not correlated with overall survival probably because salvage neck-node dissection could be effective for regional recurrence. Hypopharyngeal cancer is known to have a relatively poor prognosis. Thus, the prognosis of hypopharyngeal cancer was compared with that of other cancers, but the tumor location showed no effect on prognosis in the present study. The reason for this is unclear, but the small number of cases might have affected the results.

The present study has some limitations. First, the histology of the patients studied in the present research was all squamous cell carcinoma, and all of the patients were treated with radiotherapy (>60 Gy to GTV). Second, pulsation from carotid artery and jaw movement may affect ADC. As described in the Section 'Patients', some cases were excluded because of artifacts. We consider that effects of such artifacts were slight and did not affect the results. Third, MR imaging of the head and neck region has shifted from a 1.5-T to a 3-T system. Further studies using the 3-T system would be preferable [28].

In conclusion, ADC is an independent predictor of prognosis in HNSCC treated with radiotherapy.

Conflict of interest The authors declare that they have no conflict of interest.

References

1. Parkin DM, Bray F, Ferlay J, Pisani P. Estimating the world cancer burden: Globocan 2000. Int J Cancer. 2001;94(2):153–6.
2. Argiris A, Karamouzis MV, Raben D, Ferris RL. Head and neck cancer. Lancet. 2008;371(9625):1695–709.
3. Tanner JE. Intracellular diffusion of water. Arch Biochem Biophys. 1983;224(2):416–28.
4. Hatakenaka M, Matsuo Y, Setoguchi T, Yabuuchi H, Okafuji T, Kamitani T, et al. Alteration of proton diffusivity associated with passive muscle extension and contraction. J Magn Reson Imaging. 2008;27(4):932–7.
5. Mardor Y, Roth Y, Ochershvilli A, Spiegelmann R, Tichler T, Daniels D, et al. Pretreatment prediction of brain tumors' response to radiation therapy using high b-value diffusion-weighted MRI. Neoplasia. 2004;6(2):136–42.
6. Higano S, Yun X, Kumabe T, Watanabe M, Mugikura S, Umetsu A, et al. Malignant astrocytic tumors: clinical importance of apparent diffusion coefficient in prediction of grade and prognosis. Radiology. 2006;241(3):839–46.
7. Murakami R, Sugahara T, Nakamura H, Hirai T, Kitajima M, Hayashida Y, et al. Malignant supratentorial astrocytoma treated with postoperative radiation therapy: prognostic value of pretreatment quantitative diffusion-weighted MR imaging. Radiology. 2007;243(2):493–9.
8. Jingu K, Kishimoto R, Mizoe JE, Hasegawa A, Bessho H, Tsuji H, et al. Malignant mucosal melanoma treated with carbon ion radiotherapy with concurrent chemotherapy: prognostic value of pretreatment apparent diffusion coefficient (ADC). Radiother Oncol. 2011;98(1):68–73.
9. Chenevert TL, Stegman LD, Taylor JM, Robertson PL, Greenberg HS, Rehemtulla A, et al. Diffusion magnetic resonance imaging: an early surrogate marker of therapeutic efficacy in brain tumors. J Natl Cancer Inst. 2000;92(24):2029–36.
10. Hamstra DA, Chenevert TL, Moffat BA, Johnson TD, Meyer CR, Mukherji SK, et al. Evaluation of the functional diffusion map as an early biomarker of time-to-progression and overall survival in high-grade glioma. Proc Natl Acad Sci USA. 2005;102(46):16759–64.
11. Koh DM, Scurr E, Collins D, Kanber B, Norman A, Leach MO, et al. Predicting response of colorectal hepatic metastasis: value of pretreatment apparent diffusion coefficients. Am J Roentgenol. 2007;188(4):1001–8.
12. Mardor Y, Pfeffer R, Spiegelmann R, Roth Y, Maier SE, Nissim O, et al. Early detection of response to radiation therapy in patients with brain malignancies using conventional and high b-value diffusion-weighted magnetic resonance imaging. J Clin Oncol. 2003;21(6):1094–100.
13. Moffat BA, Chenevert TL, Lawrence TS, Meyer CR, Johnson TD, Dong Q, et al. Functional diffusion map: a noninvasive MRI biomarker for early stratification of clinical brain tumor response. Proc Natl Acad Sci USA. 2005;102(15):5524–9.
14. Kato H, Kanematsu M, Tanaka O, Mizuta K, Aoki M, Shibata T, et al. Head and neck squamous cell carcinoma: usefulness of

diffusion-weighted MR imaging in the prediction of a neoadjuvant therapeutic effect. Eur Radiol. 2009;19(1):103–9.
15. Kim S, Loevner L, Quon H, Sherman E, Weinstein G, Kilger A, et al. Diffusion-weighted magnetic resonance imaging for predicting and detecting early response to chemoradiation therapy of squamous cell carcinomas of the head and neck. Clin Cancer Res. 2009;15(3):986–94.
16. Galban CJ, Mukherji SK, Chenevert TL, Meyer CR, Hamstra DA, Bland PH, et al. A feasibility study of parametric response map analysis of diffusion-weighted magnetic resonance imaging scans of head and neck cancer patients for providing early detection of therapeutic efficacy. Transl Oncol. 2009;2(3):184–90.
17. Hatakenaka M, Nakamura K, Yabuuchi H, Shioyama Y, Matsuo Y, Ohnishi K, et al. Pretreatment apparent diffusion coefficient of the primary lesion correlates with local failure in head-and-neck cancer treated with chemoradiotherapy or radiotherapy. Int J Radiat Oncol Biol Phys. 2011;81(2):339–45.
18. Hatakenaka M, Shioyama Y, Nakamura K, Yabuuchi H, Matsuo Y, Sunami S, et al. Apparent diffusion coefficient calculated with relatively high b-values correlates with local failure of head and neck squamous cell carcinoma treated with radiotherapy. Am J Neuroradiol. 2011;32(10):1904–10.
19. Vandecaveye V, Dirix P, De Keyzer F, Op de Beeck K, Vander Poorten V, Hauben E, et al. Diffusion-weighted magnetic resonance imaging early after chemoradiotherapy to monitor treatment response in head-and-neck squamous cell carcinoma. Int J Radiat Oncol Biol Phys. 2012;82(3):1098–107.
20. Hauser T, Essig M, Jensen A, Gerigk L, Laun FB, Munter M, et al. Characterization and therapy monitoring of head and neck carcinomas using diffusion-imaging-based intravoxel incoherent motion parameters—preliminary results. Neuroradiology. 2013;55(5):527–36.
21. Ohnishi K, Shioyama Y, Hatakenaka M, Nakamura K, Abe K, Yoshiura T, et al. Prediction of local failures with a combination of pretreatment tumor volume and apparent diffusion coefficient in patients treated with definitive radiotherapy for hypopharyngeal or oropharyngeal squamous cell carcinoma. J Radiat Res. 2011;52(4):522–30.
22. Hatakenaka M, Shonai T, Aratani K, Onodera M, Nakamura K, Yabuuchi H, et al. The calculation method of ADC affects the correlation between prognosis and ADC (in Japanese). Jpn J Magn Reson Med. 2012;32(Supplement):327. http://www.jsmrm.jp/modules/en/index.php?content_id=1.
23. Hatakenaka M, Soeda H, Yabuuchi H, Matsuo Y, Kamitani T, Oda Y, et al. Apparent diffusion coefficients of breast tumors: clinical application. Magn Reson Med Sci. 2008;7(1):23–9.
24. Rzeszowska-Wolny J, Przybyszewski WM, Widel M. Ionizing radiation-induced bystander effects, potential targets for modulation of radiotherapy. Eur J Pharmacol. 2009;625(1–3):156–64.
25. Le Bihan D, Breton E, Lallemand D, Aubin ML, Vignaud J, Laval-Jeantet M. Separation of diffusion and perfusion in intravoxel incoherent motion MR imaging. Radiology. 1988;168(2):497–505.
26. Yamada I, Aung W, Himeno Y, Nakagawa T, Shibuya H. Diffusion coefficients in abdominal organs and hepatic lesions: evaluation with intravoxel incoherent motion echo-planar MR imaging. Radiology. 1999;210(3):617–23.
27. Oppo K, Leen E, Angerson WJ, Cooke TG, McArdle CS. Doppler perfusion index: an interobserver and intraobserver reproducibility study. Radiology. 1998;208(2):453–7.
28. Bou-Assaly W, Srinivasan A, Mukherji SK. Head and neck high-field imaging: oncology applications. Neuroimaging Clin N Am. 2012;22(2):285–96 (xi).

Laboratory Investigation (2015) 95, 193–206
© 2015 USCAP, Inc All rights reserved 0023-6837/15

Anterior gradient 2 downregulation in a subset of pancreatic ductal adenocarcinoma is a prognostic factor indicative of epithelial–mesenchymal transition

Yusuke Mizuuchi[1,2], Shinichi Aishima[1], Kenoki Ohuchida[3], Koji Shindo[1,2], Minoru Fujino[1], Masami Hattori[1], Tetsuyuki Miyazaki[1], Kazuhiro Mizumoto[4], Masao Tanaka[3] and Yoshinao Oda[1]

Anterior gradient 2 (AGR2), a member of the protein disulfide isomerase family, has been implicated in various cancers including pancreatic ductal adenocarcinoma (PDAC) and is known to promote cancer progression. However, the prognostic value of AGR2 expression and the interaction with epithelial–mesenchymal transition (EMT) remain unclear. We investigated the clinical significance of AGR2 and EMT markers in PDAC patients by immunohistochemical analyses. Although AGR2 expression was not observed in normal pancreas, all pancreatic precursor neoplastic lesions were positive for AGR2, even at the earliest stages, including pancreatic intraepithelial neoplasia-1A, AGR2 expression was reduced in 27.7% (54/195 cases) of PDAC patients. AGR2 downregulation correlated with EMT markers (vimentin overexpression and reduced membranous E-cadherin expression), high Union for International Cancer Control stage ($P<0.0001$), high histological cellular grade ($P<0.0001$), and adverse outcome ($P<0.0001$). *In vitro*, targeted silencing of AGR2 in cancer cells using siRNA reduced cell proliferation, colony formation, cell invasiveness, and migration, but did not alter EMT markers. To confer a more aggressive phenotype and induce EMT in PDAC cells, we co-cultured PDAC cell lines with primary-cultured pancreatic stellate cells (PSCs) and found that AGR2 was downregulated in co-cultured PDAC cells compared with PDAC monocultures. Treatment with transforming growth factor beta-1 (TGF-β), secreted from PSCs, decreased AGR2 expression, whereas inhibition of TGF-β signaling using recombinant soluble human TGF-β receptor type II and TGF-β-neutralizing antibodies restored AGR2 expression. We conclude that AGR2 downregulation is a useful prognostic marker, induced by EMT, and that secreted TGF-β from PSCs may partially contribute to AGR2 downregulation in PDAC patients. AGR2 downregulation does not induce EMT or a more aggressive phenotype, but is a secondary effect of these processes in advanced PDAC.

Laboratory Investigation (2015) **95,** 193–206; doi:10.1038/labinvest.2014.138; published online 24 November 2014

Pancreatic ductal adenocarcinoma (PDAC) is one of the leading causes of cancer death in the United States, with an overall survival rate of 3–5%.[1] Early recurrence following resection is associated with high mortality, and to date, few treatment options are available. Thus, the development of novel markers for early detection and prognosis prediction is necessary to improve the management of patients with PDAC. Understanding of the progression from precursors to invasive disease has significantly advanced, following the identification of three important precursors, including pancreatic intraepithelial neoplasia (PanIN), intraductal papillary mucinous neoplasms (IPMNs), and mucinous cystic neoplasms. However, the mechanisms underlying the progression from these precursors to invasive disease remain unclear.[2–4]

Anterior gradient genes were first identified in *Xenopus laevis* and are named according to their specific expression patterns during embryonic development.[5,6] Anterior gradient 2 (*AGR2*) homolog expression is responsible for the development of the cement gland, a glandular organ in frog embryos, and for limb regeneration in newts.[7,8] In humans, the *AGR2* gene lies at chromosomal position 7p21.3, and gives rise to an 18-kDa-sized protein. AGR2 is classified as a member of

[1]Department of Anatomic Pathology, Graduate School of Medical Sciences, Kyushu University, Fukuoka, Japan; [2]Reserch Fellow of Japan Society for the Promotion of Science, Tokyo, Japan; [3]Department of Surgery and Oncology, Graduate School of Medical Sciences, Kyushu University, Fukuoka, Japan and [4]Kyushu University Hospital Cancer Center, Fukuoka, Japan
Correspondence: Professor Y Oda, MD, PhD, Department of Anatomic Pathology, Graduate School of Medical Sciences, Kyushu University, 3-1-1 Maidashi, Fukuoka 812-8582, Japan.
E-mail: oda@surgpath.med.kyushu-u.ac.jp

Received 16 February 2014; revised 28 August 2014; accepted 22 September 2014